



EVLA Memo No. 222

Coordinated Starlink User Terminal Testing Near the VLA

Chris De Pree, Urvashi Rau, Rob Selina, Brian Svoboda, Tony Beasley

April 15, 2023

Abstract

NRAO and SpaceX have undertaken a series of coordinated radio frequency (RF) measurement tests to gauge the impact of Starlink User Terminals (UTs) uplink (14.0-14.5 GHz) and downlink (10.7-12.7 GHz) transmissions on the normal operations of the Very Large Array (VLA), the Very Long Baseline Array (VLBA) and the Green Bank Telescope (GBT). Phase I testing (September 2021) involved running the User Terminal in normal mode at a variety of locations near the Very Large Array and the Pie Town VLBA antenna. Phase II testing (October 2021) involved fixed channel downlink frequency illumination of the VLA by Starlink satellites. Initial analysis of the Phase I testing indicates that UT uplink transmissions (between 14.0 and 14.5 GHz) have minimal impact on VLA and VLBA data integrity in locations where there is no line of sight from the UT to the telescope. Phase II testing demonstrated that analytical interference models have good correlation to real world observations, and as predicted by the model, satellite downlink transmissions were detected only on some of the shortest baselines of the B configuration. The impacted baselines change (as predicted) according to the location of the transmitting satellite at any given time. As part of a pilot test, NRAO has also been installing and operating a number of UTs in Socorro County near the VLA, allowing NRAO to gauge the integrated impact of a larger number of UTs operating in the proximity of the VLA. In this memo, we present the results of the Phase I, and Phase II tests. These early coordination tests can inform future studies for the type of spectrum sharing that could be carried out in an eventual National Radio Dynamic Zone (NRDZ). Results of the pilot experiment near the VLA and GBT testing will be described in separate memos.

TABLE OF CONTENTS

1	INTRODUCTION	1
1.1	Satellite Constellations	1
1.2	The Starlink System	2
2	RFI THEORY & MODELING.....	2
2.1	Measured power levels	3
2.2	Attenuation due to the interferometer response	4
2.3	Use of telemetry files	5
2.4	Example prediction.....	6
3	COORDINATED TESTING AT THE VLA AND VLBA (PHASE I)	8
3.1	VLA - Phase I testing	8
3.1.1	Test Plan - Normal Operations	8
3.1.2	VLA Setup	9
3.1.3	Uplink and Downlink results.....	10
3.1.4	Uplink Signals	10
3.1.5	Downlink Signals.....	10
3.2	VLA - Phase II testing	13
3.2.1	Test Plan - Fixed Channel Operations.....	13
3.2.2	Downlink Results	13
3.2.3	VLA Setup	13
4	OVERALL RESULTS & CONCLUSIONS	15
5	ACKNOWLEDGMENTS.....	16
6	REFERENCES	16
7	APPENDIX A – SITE PROPAGATION PROFILES.....	17

I INTRODUCTION

Satellite transmission interactions with radio telescopes have a history that stretches back over several decades (e.g. Thompson 1982). While interactions between satellite constellations and optical observations have been more in the news in the past few years, the function of satellite constellations (transmitting and receiving radio transmissions) make them potential sources of significant radio frequency interference (RFI) for sensitive radio telescopes operating around the globe. In the past, radio observatories were often protected geographically from sources of RFI by their remote locations, specifically protected by regional set asides (e.g. the National Radio Quiet Zone), and in some cases by additional agreements forged by the NSF and FCC to protect radio astronomy services from new spectrum users in particular bands (e.g. <https://beta.nsf.gov/news/statement-nsf-and-spacex-radio-spectrum-coordination-agreement>). While Medium Earth Orbit (MEO) and Geostationary Earth Orbit (GEO) satellites have already caused observatories to change observing strategies, the advent and rapid expansion of large, Low Earth Orbit (LEO) satellite constellations have ensured that no location on the surface of the Earth is 'remote' from potential sources of radio emission.

I.1 Satellite Constellations

Prior to the launch of satellite constellations like Starlink (SpaceX), cm-wavelength radio observatories mostly had to contend with downlink frequencies in the 12.2 to 12.7 GHz range from geostationary satellites (<https://www.thespacereview.com/article/3702/1>). Figure 1 gives an example of these signals, regularly detected during RFI scans at the Jansky Very Large Array (JVLA). RFI in this frequency range can be partially mitigated by not observing at these frequencies in the southern sky (in the direction of these geostationary satellites), but for the most part, this part of the radio spectrum has become so filled with active radio transmissions that large bandwidths have to be excised in radio frequency observations in order to enable scientific research. Since many radio observatories are technically able to observe outside their narrow, protected bands, radio astronomers have long practiced the excision of data corrupted with non-astronomical signals in order to preserve the astronomical data within the observed band (e.g. Maan, van Leeuwen & Vohl 2021).

New LEO mega-constellations are licensed to utilize a range of downlink frequencies (10.7-12.7 GHz), but instead of being located in a particular band of the sky, are now located in low Earth orbits that carry them across the sky in tens of minutes, as seen from most locations on the planet's surface. For these reasons, the downlink signals are much harder, if not impossible, to avoid without coordination.

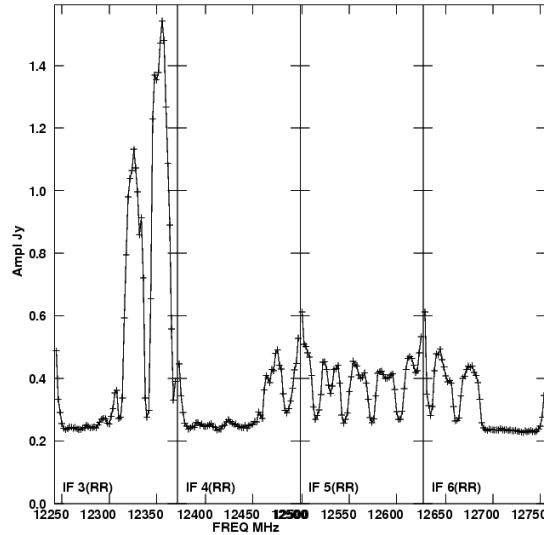


Figure 1: Sample of Ku Band RFI from along the geostationary orbit (GSO) belt. This plot is an integrated spectrum made from a 1-minute observation with the Very Large Array in NM while pointed at the north celestial pole (NCP). This static position on sky is chosen to permit the averaging of the power spectral density received from RFI sources without the impact of interferometric attenuation from fringe winding.

1.2 The Starlink System

SpaceX began launching production Starlink satellites in late 2019 and shipping Starlink User Terminals (UTs) in quantity in 2021. Starlink uses 500 MHz from 14.0-14.5 GHz for their UT uplinks, and ~2 GHz (10.7-12.75 GHz) for their UT downlinks. Uplink UT signals use one of 8 (62.5 MHz) channels in that range, with all UTs in a given cell sharing the same uplink channel. During normal operations, all Starlink UTs in a given cell will dynamically switch uplink and downlink channels. Uplink transmissions use 60 MHz of each 62.5 MHz channel. The UT emissions towards the horizon are limited to -72.76 dBW/Hz in 60 MHz, which corresponds to a maximum equivalent isotropic transmitter power of approximately 3.2 W.

Downlinks are transmitted in one of eight (250 MHz) channels. The highest equivalent isotropically radiated power density (-15.0 dBW/4kHz for satellites in 570 km orbits) occurs at maximum slant (40.5 degrees from nadir). Starlink satellites adjust transmitting power using phased array beams, accounting for spreading loss and transmitting antenna gain to achieve a target power flux density (PFD) at each UT of -146 dBW/m²/4 kHz. The UT can transmit with a maximum short-term duty cycle¹ of 33%, although the long-term duty cycle is limited to 11% over 30 minutes (this is a radiation hazard requirement). In practice, the duty cycle is typically of the order of 1% or less, depending on network traffic.

For reference, Starlink's downlink 250 MHz wide channels start at the following frequencies: 10.7, 10.95, 11.2, 11.45, 11.7, 11.95, 12.2, 12.45 GHz, and uplinks are between 14.0 and 14.5 GHz.

2 RFI THEORY & MODELING

Understanding the impact of satellite constellation transmissions on radio astronomy observations is a key element of any predictive strategy to minimize impact on observatory operations. As part of our coordinated Starlink tests, we are creating a model of the interferometer response to user terminals and satellites and validating it against the observed data. Two parts of the model are discussed below. The first

¹ This is the percentage of the ratio of pulse duration, or pulse width to the total period of the waveform.

estimates the spectral power flux density measured at each antenna, based on a comparable model developed for the ngVLA (Selina, 2021), and the second provides the expected interferometer response to such signals.

2.1 Measured power levels

The measured spectral power flux density (SPFD, $W/m^2/Hz$) has been computed for possible pairings of transmitter and receiver main lobes and side lobes. For Starlink satellite transmissions, the documented power flux density (PFD) at the Earth’s surface is $-146 W/m^2/4kHz$ (ECC Report 271), with a satellite forward (main lobe) gain of 38.3dB relative to a 0dBi sidelobe gain.

Depending on the direction of downlink transmission, the transmitter gain is either through the main lobe or a side lobe. A user terminal has an effective isotropic radiative power (EIRP) of 3.2 W and we assume that only UT sidelobes (gain = 0dBi) will be visible from a radio telescope, since communications links are only established at elevations of 49.5 degrees or higher relative to each UT. The receiver forward gain is computed for a 25m VLA dish as $10\log_{10}k(\pi D/\lambda)^2$ dB relative to a 0dBi sidelobe gain, where D is the telescope diameter (m), λ is the observing wavelength (m), and k is the antenna efficiency. The antenna gain as a function of angular distance from the pointing center is computed using an Airy disk model, leading to sidelobe gains that vary between +2dB for the near-in sidelobes to -20 dB for the far-out sidelobes.

Table I shows the calculated SPFDs for both satellites and User Terminals in the case of Satellite (main lobe and side lobe) and UT (side lobe) interactions with the VLA (main lobe and side lobe). We assume that given the small size of the VLA main lobe and the rapid movement of satellites across the sky, a main lobe (VLA) to main lobe (satellite) interaction will be exceedingly rare. In particular, the location of the VLA (and other radio telescopes) does not receive main beam illumination from any SpaceX satellites during normal operations, thanks to SpaceX implemented exclusion zones, so that the most likely interaction will be satellite sidelobe to VLA sidelobe (see Table I).

	SAT Mainlobe W/m²/Hz	SAT Sidelobe W/m²/Hz	UT Sidelobe W/m²/Hz
VLA Mainlobe	-182 dB [6e+7 Jy]	-220 dB [9e+3 Jy]	VLA will never point at a UT
VLA Sidelobe	-248dB [15 Jy] : inner -275dB [0.05 Jy] : outer	-286 dB [2e-03 Jy] : inner -313 dB [4e-06 Jy] : outer	-253dB [4 Jy] at 50km -246dB [25 Jy] at 20km -200dB [1e+6 Jy] at 0.1 km

Table I: Predicted received SPFD from Starlink Satellites and User Terminals with the Very Large Array for permissible combinations of antenna main lobes and sidelobes.

The maximum received power of 6e+7 Jy is generally above the receiver saturation limit but well below the input damage threshold for the LNAs. As noted previously, a mainlobe-mainlobe interaction is itself highly unlikely, given that the cells around the VLA are excluded from main beam illumination and only one satellite per constellation operator illuminates a cell at a given time. The most commonly expected situation is a sidelobe-sidelobe interaction with power levels that may be undetectable in individual measurements.

It is worth noting that the expected power levels from ground-based UT sidelobes are anticipated to be higher than the satellite mainlobes for distances out to 20km when the UT sidelobes are in line-of-sight to the VLA antenna. Interferometric attenuation will play an important part in determining the relative risk associated with these signals and observing scenarios.

Our coordinated Phase II tests with Starlink (described in later sections) tested the VLA sidelobe and SAT mainlobe combination, with a cell over the VLA being illuminated while the VLA was pointed at a calibrator source several degrees away from the satellite at any time.

2.2 Attenuation due to the interferometer response

A radio interferometer tracks a fixed position on the sky by continuously adjusting the expected relative phase between all antenna pairs (or baselines) to be zero for that phase tracking center. Signals from any source of emission located away from the phase tracking center incur a non-zero sinusoidal relative phase which carries information about the source position at any instant in time. If this source is located far enough away from the phase center, or is moving relative to the sky, the non-zero and time-varying relative phase results in an attenuation of the correlated signal due to the non-zero time and frequency range over which the signals are averaged, per measurement.

Thompson (1982, 1999) and Perley (2002) describe this effect for a geostationary satellite. Here, we extend this analysis to a source of RFI (e.g. a satellite) moving in an arbitrary (but known) direction.

Interferometric attenuation occurs as a result of time averaging as well as bandwidth decorrelation, and we estimate the effect of each separately.

The amount of attenuation due to time averaging, per baseline, is given by $R = \text{sinc}(\pi\nu_f t)$ where ν_f is the natural fringe frequency and t is the integration time. Since the relative phase between two antennas changes by 2π when w changes by one wavelength, a fringe frequency may be calculated as $\nu_f = dw/dt$, where u, v, w are related to the antenna locations L_X, L_Y, L_Z as per Eqn 2-30 of Thompson 1999.

Allowing for arbitrary satellite motion with $\omega_H = dH/dt$ and $\omega_\delta = d\delta/dt$ we get

$$\nu_f = \omega_\delta \nu_s - \omega_H u_s \cos \delta_s$$

A fringe frequency due to Earth rotation alone (Eqn 2-32 of Thompson 1999) is given by $\nu_f = \omega_e u_\phi \cos \delta_\phi$ by setting $\omega_H = \omega_E$, and $\omega_\delta = 0$ in the above equation, and where ϕ represents the phase center.

For our analysis, we are interested in the relative phase difference and fringe frequency between the phase center direction (H_ϕ, δ_ϕ) and the satellite location (H_s, δ_s). This is given by

$$\nu_f = \omega_\delta \nu_s - \omega_H u_s \cos \delta_s + \omega_e u_\phi \cos \delta_\phi$$

For a satellite in a polar orbit, $\omega_H = 0$. For a satellite in an equatorial orbit, $\omega_\delta = 0$, and for a geostationary source of RFI, $\omega_H = 0$ and $\omega_\delta = 0$. A celestial source moving with the phase tracking center may be represented by $\omega_H = \omega_e$ and $\omega_\delta = 0$.

The amount of attenuation due to bandwidth decorrelation, per baseline, is given by

$$R = \text{sinc}(\pi\beta\tau_d)$$

where β is the observing bandwidth and τ_d is the difference in delay between the phase center direction and the source of interference (Eqn 18 of Thompson 1982).

For a single baseline, the combined attenuation is given by the product of the two terms. In our model, we calculate the attenuation for each baseline in the array, for a series of timesteps. Satellite locations and

speeds along the H and δ axes are approximated from telemetry information supplied by SpaceX. UTs are treated as stationary objects with a relative fringe rate given by the Earth rotation speed ($0.004^\circ/\text{sec}$).

The VLA B-configuration was used in these tests with the geometry and attenuation calculated for source and satellite locations at a series of time intervals within a chosen 5-minute scan. In addition, an Airy disk model was used to compute the VLA antenna gain at the angular distance between the phase center and satellite locations for each time interval. This gain was multiplied with the received power (see previous section) prior to applying the interferometric attenuation. For our test observations, the angular distance between the satellite(s) and the phase tracking center varied between 10 and 40 degrees.

Our initial model predicts a median attenuation of 30-40 dB across all baselines with the longest baselines seeing up to 50 dB attenuation.

2.3 Use of telemetry files

SpaceX has provided satellite telemetry files for all of the test runs described in this memo. These datasets are extremely useful in establishing the expected signal strength on a particular baseline for a particular transmission time. Figure 2 shows the transmitting satellite locations for five minutes of our Phase II test, projected onto a tangent plane at the VLA site. The telemetry data is used to predict the interferometric attenuation with the model which can then be compared to the visibility data in the measurement set.

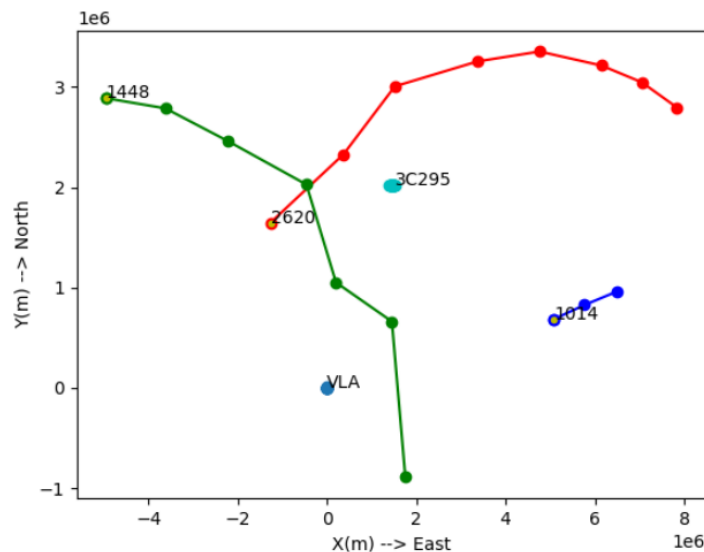


Figure 2: Satellite locations for a five-minute scan during the Phase II test where the VLA cell was constantly illuminated by downlink signals in Channel 4 ($\sim 11.45 - 11.7$ GHz). The satellite tracks and source positions are shown projected onto a tangent plane at the VLA site, with the VLA apex at the origin. This data enables an assessment of the interferometric response to the moving satellites given the orientation for each baseline pair in the array.

At an altitude of 570 km, corresponding to the Starlink satellites in this test, LEO satellites are completing a full revolution around the earth every ~ 5755 seconds (~ 96 min). Approximately 46.76 degrees of their orbit is above the local horizon, and they traverse that distance in 748 sec (12.5 min), so their average angular rate of motion from the interferometer reference frame is $= 0.0042$ rad/sec ($0.24^\circ/\text{sec}$). Peak rate at Zenith can be approximately $0.76^\circ/\text{sec}$ and decreases towards the horizon, roughly consistent with the telemetry data.

The satellite speed along the H and δ axes were also approximated from the telemetry files. The speed along the DEC axis ranged between -0.5 and $+0.5^\circ/\text{sec}$, and the speed along the HA axis ranged between -0.5 and $-1.2^\circ/\text{sec}$ across the 5 minute scan being analyzed.

2.4 Example prediction

We use the telemetry data associated with the Phase II test from Figure 2 to predict the magnitude of the PSD from a Starlink satellite intentionally illuminating the VLA site on a per-baseline basis as a function of time. To aid the reader, the more familiar spectral flux density unit of Jansky is used, where $1 \text{ Jy} = 10^{-26} \text{ W/m}^2/\text{Hz}$.

Figure 3 (left) shows the predicted visibility amplitude (SPFD measured per baseline) for a VLA sidelobe and satellite mainlobe interaction at one instant in time. The geometry was chosen to approximate the conditions within the 45 second time range of a clear RFI detection during one five-minute scan of our Phase II tests. Only a few short baselines, where projection effects minimize interferometric attenuation, are expected to show amplitudes at or near the $\sim 10 \text{ Jy}$ level projected in Table 1. All other baselines are expected to measure a lower amplitude, due to attenuation. The effect of satellite signals seen at amplitudes lower than the single baseline noise level, but higher than the expected image rms level, can be best analyzed by imaging tests that check whether or not theoretical rms levels are reached. These types of imaging test have been performed in the pilot monitoring datasets (De Pree et al., 2023).

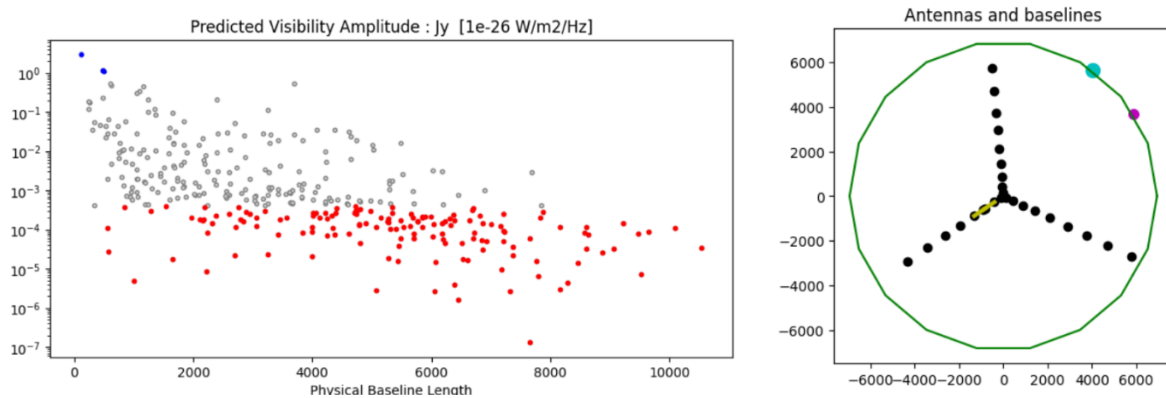


Figure 3: Example: Predicted visibility amplitude for one instant in time. The right panel shows the VLA array configuration, the azimuth locations of the phase tracking center (blue) and a satellite (magenta), and baselines for which the predicted satellite signal amplitude are strongest are shown in yellow. The left panel shows the predicted visibility amplitude across baseline length. The points in blue are the strongest (above the source brightness for our Phase II test) and correspond to the baselines marked in yellow on the right panel. The grey points are visibilities that are below the source brightness (for this particular test) but still above the image noise level. The red points represent the data points below a fiducial theoretical image rms level.

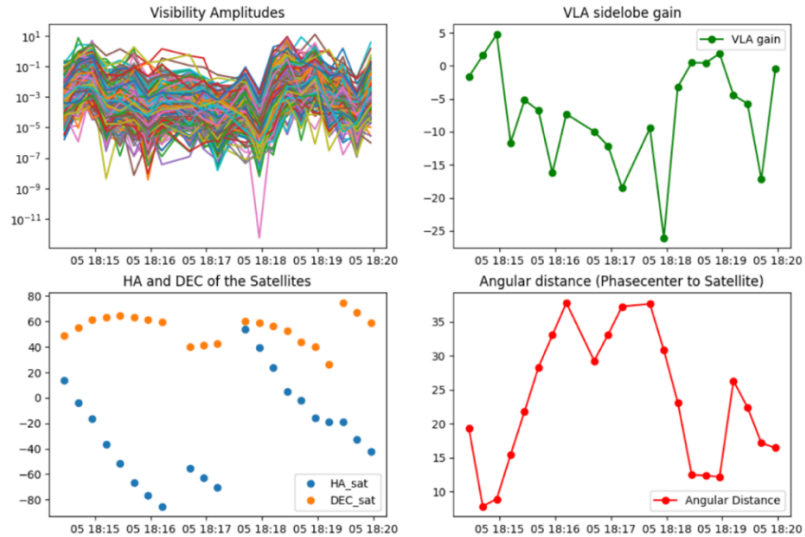


Figure 4: The top left panel plots the predicted signal amplitude at any time during the five-minute scan corresponding to the satellite tracks in Fig.2. The colors depict different baselines. The bottom left panel shows the hour-angle and declination of the satellite tracks. Discontinuities in the satellite hour angle (HA) and declination (DEC) plot are the result of a downlink satellite change at this time. These changes in transmitting satellite location have predictable effects on the projected baseline geometry and resulting interferometric attenuation, but this pattern is overshadowed by the VLA antenna gain. Such variations suggest that that different short baselines will be flagged at different times during a typical length scheduling block. The top right panel illustrates the VLA sidelobe gain (in dBi) assumed for all antennas, and the bottom right panel shows the angular distance (in degrees) between the phase tracking center and the satellite. A larger angular distance corresponds to a lower sidelobe gain level.

Figure 4: shows the predicted visibility amplitude for a series of timesteps within the 5-minute scan chosen for detailed analysis, along with the satellite Hour-angle and Declination, the angular distance between the phase tracking center and the satellite and the resulting VLA antenna sidelobe gain used in the model.

Finally, it is important to note various assumptions in these model estimates. We assume that all antennas see equal power levels with the same Airy disk sidelobe pattern and receiver gain, and that the transmitter is in the far-field of the interferometer. However, in reality, power levels from some sources may vary across the array and the sidelobe gain through which each antenna sees an RFI source is likely to vary considerably from antenna to antenna. For moving satellites, we use an approximate speed estimated from the telemetry information. At each integration, we assume that the median SPFD is equivalent to the amplitude at which a source might appear in a calibrated image, and make comparisons with theoretical image noise levels to assess whether or not one should see imaging artifacts or a noise floor. Of course, the difference in attenuation across baselines and arbitrary beam sidelobe gains would break this assumption and would decrease the degree of coherence in the measured signal. De Pree et al. (2023) estimates the effect on imaging.

The simulation results presented above are compared to the measured Phase II test results in subsequent sections. These simulation results are quite hopeful, suggesting that imaging the downlink band even with a Starlink satellite illuminating the VLA site could be possible (with a significant fraction of data flagged on short baselines). Accounting for the 38dB difference in satellite mainlobe vs sidelobe gain suggests that Starlink satellites illuminating other locations in normal operations should result in minimal data flagging. When looking at Figure 3, for example, the resulting visibility amplitudes would drop by 6×10^3 , with most measurements below the imaging noise floor. Although this result is consistent with findings in the Phase I tests described in the following section, we must interpret this with appropriate caution as this

experiment does not yet place any bounds on a noise floor that might be reached when imaging in the presence of such partially decorrelated RFI.

3 COORDINATED TESTING AT THE VLA AND VLBA (PHASE I)

Since Fall 2021, NRAO and SpaceX have cooperated to perform a series of tests of the impact of Starlink User Terminal (UT) uplink and downlink transmissions on the normal operations of the Very Large Array and VLBA. Tests in New Mexico were performed in September (Phase I) and October (Phase II) 2021, and are described in detail below.

Data were collected on the shortest baselines to the VLBA Pie Town antenna at the time of the September (Phase I) tests. While visible in autocorrelation spectra, no interference in cross-correlated measurements with the VLBA Pie Town antenna was detected during this test, which is consistent with the expected attenuation on these VLB-scale baselines.

3.1 VLA - Phase I testing

The first set of tests were carried out during the September VLA move from C- to B-configuration, during September 15-17, 2021. SpaceX provided a UT device, and a SpaceX representative was present for the testing. The UT (0.48 m diameter) required portable power to operate in remote locations, which was provided by an inverter powered by one of two vehicles involved in the testing. Test locations included several cities and towns near the VLA (e.g. Socorro, Magdalena and Datil), as well as two locations in the nearby Alamo Navajo Reservation. Continued testing from UTs located at the Alamo site tests are ongoing, and described in a separate Memo (De Pree et al. 2023).

3.1.1 Test Plan - Normal Operations

The main goal of these tests was to assess the impact of a UT operating normally near the VLA on typical data acquisition. The UT and SpaceX satellites were operating normally. As the location of the UT changed from site to site, SpaceX updated their database so that satellites could communicate with the UT. The variety of locations chosen were to assess the impact of UT location (both uplink and downlink signals) on the sensitive receivers of the VLA.

Location Code	Location	14 GHz Emission Detected	UL Signal Detected	DL Signal Detected	Comments/Notes
I.1	VLA Site	Y	Y	N	Restarted <i>iperf3</i> command at 6:31 to saturate downlink. Narrow band signal only detected with UT "on". ~60 MHz uplink signal detected.
I.2	Route 60 toward Magdalena	Y	N	N	Saturated uplink for 10 min, downlink for 10 min. Narrow band signal detected with UT "off" and "on". Narrow band signal at 14.28125 GHz detected during startup (see Figure 7).
I.3	Magdalena	N	N	N	Tried to saturate both uplink and downlink simultaneously with two terminal windows. This did not work. At 12:01 changed to saturating downlink only.

Location Code	Location	14 GHz Emission Detected	UL Signal Detected	DL Signal Detected	Comments/Notes
1.4	Socorro (Site 1)	N	N	N	Tried 7 min UL and 13 min DL. DK lost Linux connection. CD started UL with ~1 minute to spare at UL frequency. DL started ~27 min into this script. Lost connection for ~2 min during DL.
2.1	Socorro (Site 2)	N	N	N	Cell not enabled by SpaceX. VLA took data, but UT not operating.
2.2	Alamo (Site 1)	Y	N	N	Planned to run UL for 7 min, DL for 13 min. UL iperf test not started until 8:52. Narrow band signal detected with UT "off" and "on", but at different frequencies.
2.3	Alamo (Site 2)	Y	N	N	Planned to run UL for 7 min, DL for 13 min. UL iperf test started 2 min late (satellite connection). Narrow band signal detected with UT "off" and "on", but at different frequencies.
2.4	Datil	Y	N	N	No issues. Narrow band UL signal detected with UT "off".
2.5	Pie Town	Y	N	N	Cell was not enabled by SpaceX (cell had been previously flagged). Down to the wire for the start of observations, but once the cell was enabled, no issues.
3.1	Socorro (Site 2)	N	N	N	No issues. Redo of 2.1 (above).

Table 2: UT positions for the Phase I VLA testing carried out September 15-16, 2021. Right column indicates notes taken during the testing. Note that these tests were successful in detecting RFI, but (aside from the VLA site, 1.1) not successful in correlating detected RFI with telemetry data provided by SpaceX.

3.1.2 VLA Setup

The VLA correlator was set up to monitor four 896 MHz portions of the spectrum, centered at approximately 11 GHz, 12 GHz, 13 GHz and 14.25 GHz. These observing bands allowed us to detect the downlink (10.7-12.75 GHz) and uplink (14.0-14.5 GHz) signals to and from the UT and any impact on observing. Each of these observing bands had seven of the same sized sub bands (128 MHz) and the same spectral resolution (1024x125 kHz channels) that is used in the current periodic VLA RFI scans.

As a result of this setup, the Phase I SpaceX test data are directly comparable to the RFI scans that have been regularly run and archived on the NRAO website beginning in 2011. At each test position, the VLA was pointed first at the calibrator source 2005+778, and data was collected with 1 second integration times in spectral line mode². Current regular RFI scans cover 1 GHz in each 1 min scan. In the Phase I tests, we collected data in each transmitter position for 45 minutes total: 5 minutes at each of the four 896 MHz wide bands (20 min total) while the UT was transmitting, and for 10 minutes (total) when the UT was not transmitting (2.5 minutes centered at each frequency: 14.25 GHz, 11 GHz, 12 GHz and 13 GHz). There was also a 5-minute scan (centered at 14.25 GHz) during the time when the UT was self-calibrating and situating itself, and 10 minutes at startup when the VLA was slewing into position. In this way, we were able to look at both uplink and downlink frequencies at times when the UT was active, and when it was not.

² This mode allows the collection of data in narrow frequency channels over a larger frequency range.

3.1.3 Uplink and Downlink results

In general, the Phase I tests from the various locations were successful in terms of signal detection. In the two locations closest to the VLA, we did detect ground-based uplink UT signals that coincided with times when we knew the UT was transmitting. Downlink signals were, however, more elusive for several reasons, including: the way in which interferometers filter RFI (see Section 2 above), the rapid movement of the Starlink satellites across the sky ($\sim 0.76^\circ/\text{sec}$) and the rapid switching between satellites and channels that happens in normal operations of the Starlink satellites. Telemetry files provided by SpaceX allowed for close comparison between times and frequencies of known downlink signals and data from the VLA.

We note that in the Phase I tests, there was a large discrepancy between the predicted and detected uplink signal strength. This is likely because the modeled UT uplink signal strength does not include propagation losses due to line of sight obstructions (see Appendix A), combined with some uncertainty in the UT sidelobe levels. However, our predicted downlink signal strength (especially in the Phase II testing described below) was relatively accurate, to within $\sim 30\%$ for the shortest baselines.

3.1.4 Uplink Signals

In the Phase I test, we made a clear detection of RFI in the uplink band with the VLA at two frequencies and times that correspond with telemetry from SpaceX (see Figure 5). Uplink signals had flux densities of up to a few Jy when they were detected. This detection was made when the UT was placed at the turnout along highway 60 near the North arm tracks that cross the highway, in clear line of sight to the VLA. Other narrow band RFI detected at this location may or may not be associated with the UT. More typical were the results from Socorro (see Figure 6) where there is no apparent correlation between SpaceX telemetry and RFI signal from the UT. We have also detected narrow band RFI signals in the uplink band at several other locations (e.g. Figure 6), but it is not clear that these detections are necessarily associated with the UT³. Figure 7 shows this same result in a different way, showing an amplitude versus frequency plot of the visibility data for the uplink channels with the UT deployed in Socorro. Figure 7 shows data from all baselines, with the two colors indicating that the UT is off (green) and on (blue).

3.1.5 Downlink Signals

While RFI was apparent across the 11.2 – 12.7 GHz range (covering SpaceX Channels 3-8, where we might expect to detect downlink signals), none of the detected RFI was clearly associated in time, frequency and/or bandwidth with the known downlink transmissions provided in the SpaceX telemetry file. Since a number of commercial satellite companies utilize the same downlink frequencies, the only conclusion we could make from the Phase I tests was that we did not detect signal correlated with SpaceX satellite telemetry and channel usage. As a result of these initial tests, we planned a follow-up test where SpaceX specified a fixed downlink frequency for the test and illuminated the VLA site. We report on the results of this Phase II test next.

³ We thought at first that some of the narrow band signals at 14.28125 GHz might have been associated with a calibration carried out by the UT during its startup sequence. Further discussion with SpaceX engineers indicates that those signals do not arise from the UT.

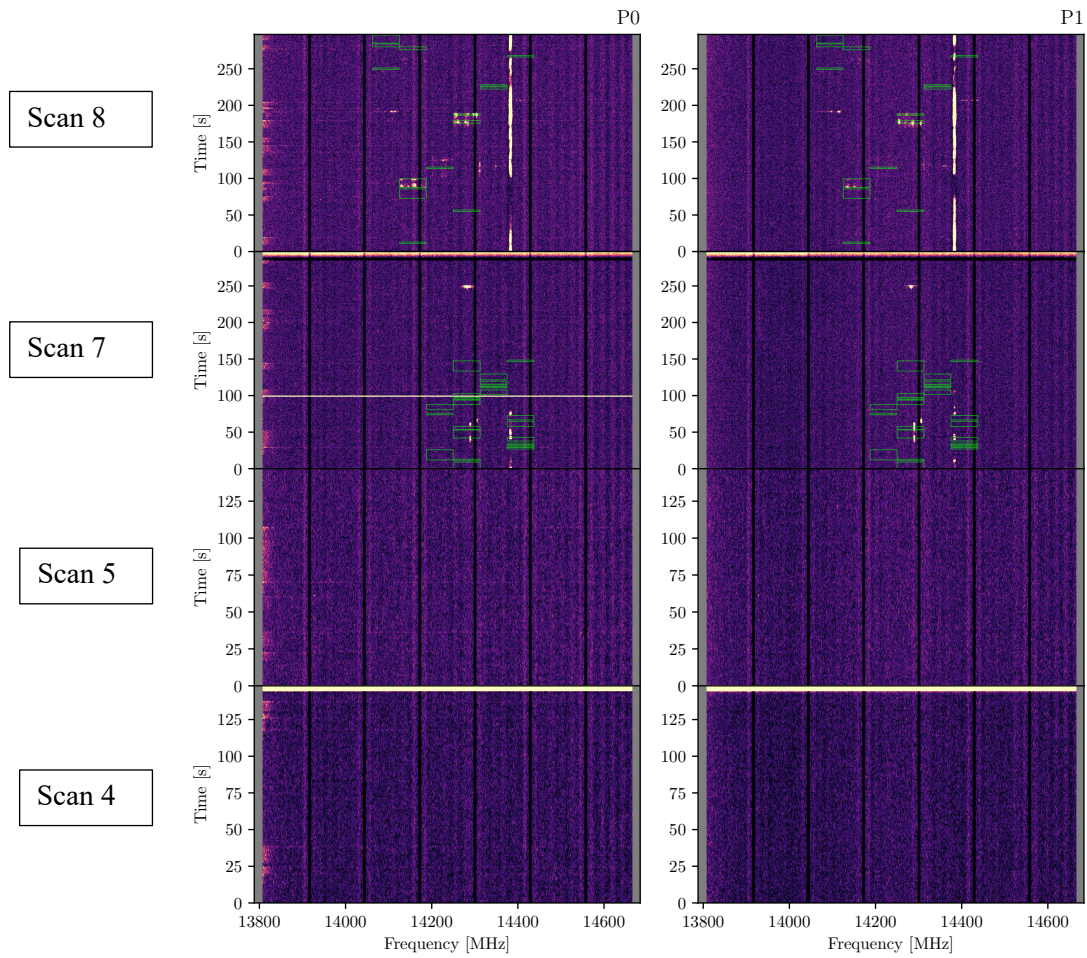


Figure 5: VLA Site (position 1.1). Detection of the uplink signal at position 1.1. Cross-correlated data from the ~20 baselines with (u,v) -distances less than 700 meters are shown. Frequency in the uplink band (14-14.5 GHz) is on the x-axis, and time is on the y-axis. Time is within scans, from bottom to top (4: UT off – VLA slewing to source, 5: UT off – VLA on source, 7: UT startup, 8: UT on – VLA on source). The green boxes (in frequency and time) are taken from the SpaceX telemetry data, indicating times when the UT was communicating with a satellite at the given frequency.

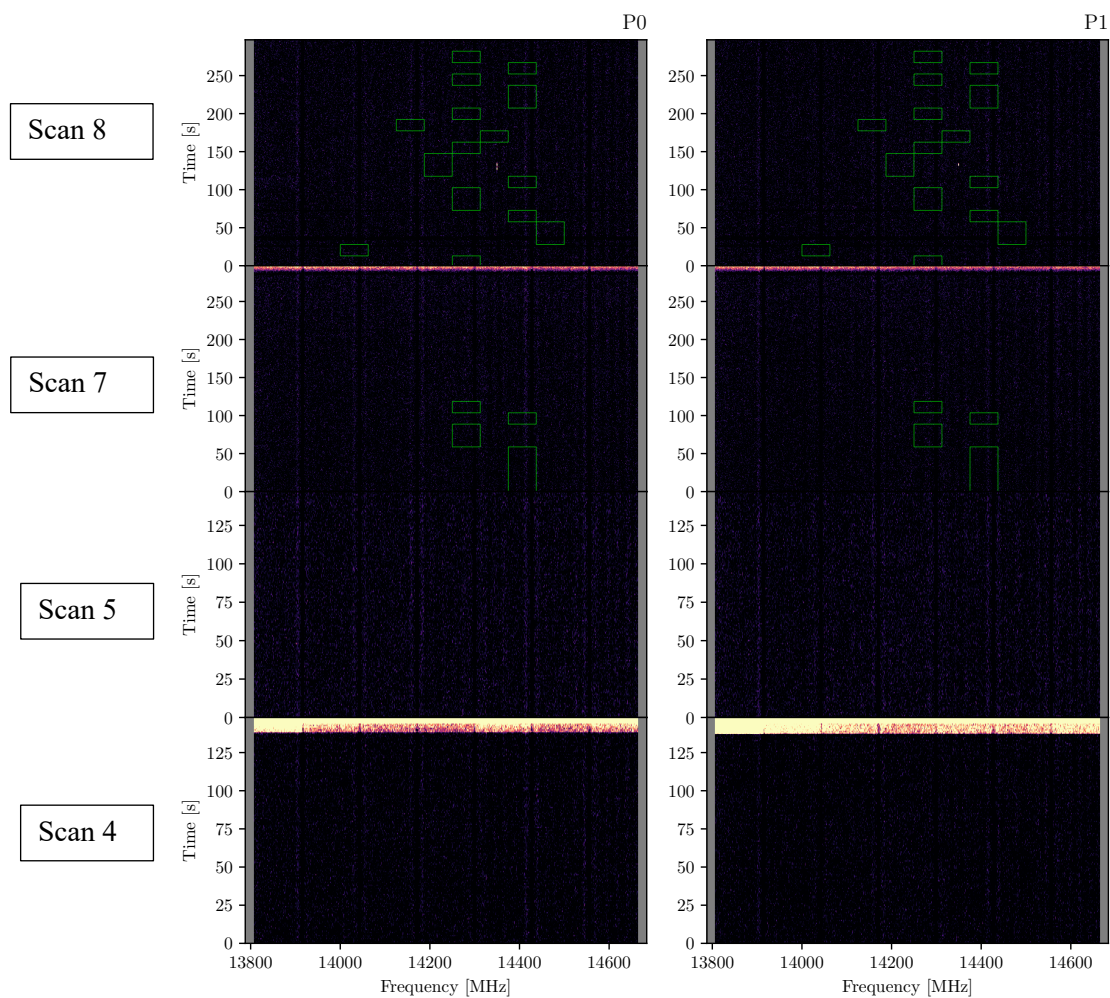


Figure 6: Socorro (position 1.4). Cross-correlated data from the ~20 baselines with (u,v) -distances less than 700 meters are shown. Frequency in the uplink band (14-14.5 GHz) is on the x-axis, and time is on the y-axis. Time is within scans, from bottom to top (4: UT off – VLA slewing to source, 5:UT off – VLA on source, 7:UT startup, 8: UT on – VLA on source). The green boxes (in frequency and time) are taken from the SpaceX telemetry data, indicating times when the UT was communicating with a satellite at the given frequency.

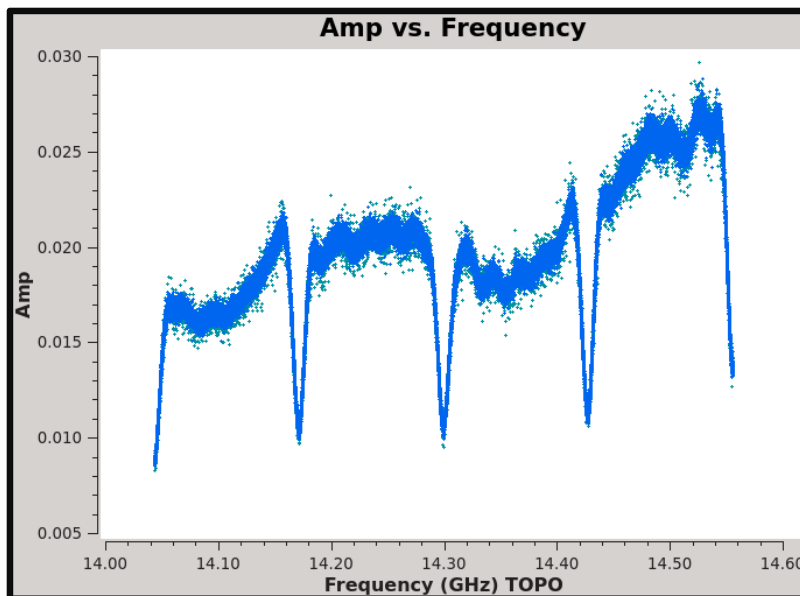


Figure 7: Non-detection of the uplink signal from the UT at position 1.4 (Socorro-Clarke Field). The green data were taken by the VLA with the UT off (Scan 4), and the blue data were taken with the UT on (Scan 7). All baselines are shown in this plot. X-axis is frequency. The data shown are from the 4 sub bands corresponding to the 8 available UT uplink frequencies between 14.0 and 14.5 GHz. These data have not been bandpass calibrated, and band edges (downturns) are apparent.

3.2 VLA - Phase II testing

The second set of tests were carried out about a month later when the VLA was in the B-configuration, on October 21, 2021. For this test, a single Starlink cell (containing the VLA) was utilized, and the UT was not used.

3.2.1 Test Plan - Fixed Channel Operations

The primary goal of this second test was to more easily identify Starlink downlink transmissions in the Ku band and to provide an indication of power levels should a LEO constellation operator illuminate an antenna site (not all constellations presently permit beamforming). For this test, the Starlink system was manually set by SpaceX engineers to transmit (from whatever satellite was serving the cell at the time) with only Channel 4 (~11.45-11.7 GHz). For this reason, any detected signal in that frequency range could be more easily associated with downlink transmissions from a particular Starlink satellite in a particular part of the sky (see description in Section 2 above). These data should be particularly helpful in the ongoing refinement and verification of the models described above.

3.2.2 Downlink Results

In these tests, we were able to clearly identify downlink transmissions and even to associate signals detected on particular baselines with transmissions from a particular satellite (see Figure 8). Detected downlink signals shared the following characteristics: (1) they were detected on short baselines, (2) they were detected in Channel 4 (frequency above), and (3) they were detected for a short period of time on that baseline, in general, for about 40 seconds.

3.2.3 VLA Setup

For the Phase II test we observed 3C295 for 17 five-minute scans. We configured WIDAR with a 1 s visibility integration time and channel resolution of 0.5 MHz in dual-polarization mode. Since only downlink signals needed to be detected, we used two 1024 MHz-wide basebands centered at 11.0 GHz and

11.99 GHz with eight 128 MHz-wide subbands each for a total of 2048 MHz bandwidth ranging from 10.49 GHz to 12.5 GHz.

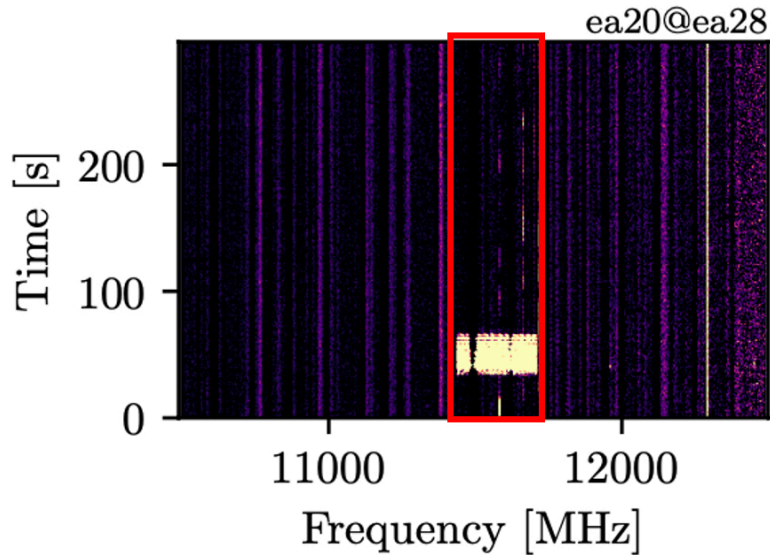


Figure 8: In this time versus frequency (waterfall plot), frequency is on the x-axis, and time is on the y-axis (increasing up), and correlated signal strength is plotted. This plot shows amplitude data from a single baseline pair of antennas, and in this case is from antennas 20 and 28. The frequency bounds of Channel 4 are indicated in red. The strongest RFI is detected at around 40 seconds from the beginning of the scan. This strong RFI occurs at the time when a switch happens from a satellite at an elevation of below 48 degrees (S2042) to an elevation of 79 degrees (S1010). The e20-e28 baseline is one of the shortest projected baselines in this configuration.

Figure 9 shows a close correspondence between the amplitude (in Jy) of the observed calibrated satellite signal on the shortest baselines, and the predicted value of approximately ~ 10 Jy from Table I and Figure 4. We note that in Figure 9, all data are shown, with only the shortest baselines detecting the satellite signal, elevated above the source signal. These results are broadly consistent with the model results depicted in Figures 3 and 4.

Imaging tests were also performed to assess the impact of satellite signals at levels below the single baseline noise but above the image rms level (grey data points in Figure 3). Due to an unrelated observational error (gain compression), these results were inconclusive. We have since been able to avoid the problem in subsequent tests reported in De Pree et al. (2023). We have not yet repeated a targeted Phase II type test with an explicit coordinated VLA cell illumination. We hope to repeat such a test in the future, perhaps in the next VLA D configuration. The monitoring tests described in De Pree et al. (2023) shows the results of this imaging analysis. Despite this issue in our first tests, the detection of interference at expected levels on short baselines was a useful outcome.

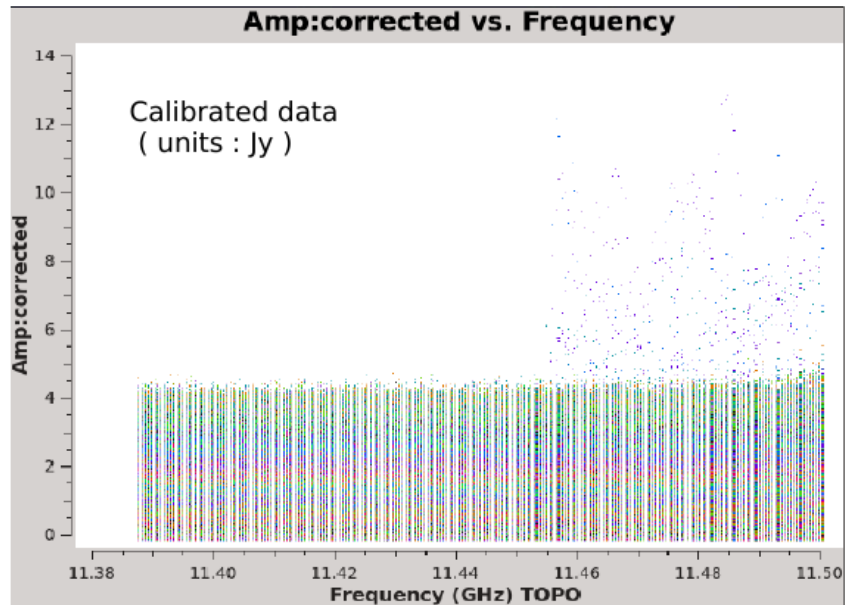


Figure 9: This plot shows calibrated visibilities at the low frequency “edge” of Starlink’s Channel 4. The satellite transmissions are seen in the top right section of the plot, corresponding to the bright region of detection in Fig.8. The calibrated amplitude is within the 7-11 Jy range which is consistent with predictions of ~ 10 Jy on the shortest projected baselines (as predicted by the model and summarized in Table 1).

4 OVERALL RESULTS & CONCLUSIONS

Early testing of Starlink User Terminals in the proximity of the VLA provide lessons for further study and improvement. In general, UT uplink signals between 14.0 and 14.5 GHz do not appear to meaningfully disrupt telescope operations, especially when there is not line of sight from the UT to the telescope. Even with a UT at the VLA site (at the Hwy 60 turnout) the broad band uplink signals were not readily detected. Narrow band signals that appear to arise from the transmitting UT (only when there is line of sight to the telescope) are still being investigated. Downlink signals are clearly detected at the VLA when in direct illumination of the cell that includes the telescopes (main beam illumination) on short baselines (e.g. Figure 8).

In the case of the VLA, the predicted downlink signal strength (on short baselines) roughly matches the detected signal, although the model does not yet correctly predict the exact baseline where the signal detection will occur. Long baselines, as expected, do not appear to suffer significant interference from the Starlink satellite downlinks. Although the downlink signal was not detected on long baselines, we do not yet have conclusive proof of whether or not the low power RFI causes a noise floor that would limit the imaging sensitivity. De Pree et al. (2023) begins to address impact to imaging for short time duration imaging (a few 10s of mins).

While we detected RFI in the VLBA-Pie Town antenna autocorrelations, we did not detect uplink or downlink signals with baselines to the VLBA-Pie Town antenna, which is not unexpected given the long baselines of the VLBA.

We anticipate future testing of coordination schemes with SpaceX and other mega-constellation operators, and are working to develop techniques that will be generally usable by both radio observatories and satellite operators for spectrum coordination.

5 ACKNOWLEDGMENTS

The authors would like to thank James Robnett and Dave Schafer (NRAO) who were instrumental in the UT testing that occurred at the VLA, and multiple colleagues for useful discussions about the model geometry and its implications. We also wish to thank SpaceX for their technical support and ongoing collaborations on coordinated testing.

Software: This research has made use of the following software projects: Astropy(The Astropy Collaboration et al. 2018), Matplotlib (Hunter 2007), NumPy and SciPy (Oliphant 2007), Pandas (McKinney 2010), IPython (Pérez & Granger 2007), CASA (CASA Team 2022), and the NASA's Astrophysics Data System.

Code used for the power level and attenuation predictions: <https://gitlab.nrao.edu/rurvashi/impact-of-satellite-rfi/>

6 REFERENCES

De Pree, C. G., Rao, U., Selina, R., Svoboda, B., Beasley, A. "SpaceX-VLA Alamo Pilot Testing", EVLA Memo 223, April 2023

Hunter, J. D. 2007, *Computing In Science & Engineering*, 9, 90, doi: 10.1109/MCSE.2007.55

McKinney, W. 2010, in *Proceedings of the 9th Python in Science Conference*, ed. S. van der Walt & J. Millman, 51 – 56

Oliphant, T. E. 2007, *Computing in Science & Engineering*, 9

Perley, R. "Attenuation of Radio Frequency Interference by Interferometric Fringe Rotation" EVLA Memo #49, November 2002

Selina, R. 2021, 'Antenna Requirements for Mitigation of LEO Constellations', ngVLA project memorandum 020.10.25.00.00-0004-MEM

The Astropy Collaboration, Price-Whelan, A. M., Sipőcz, B. M., et al. 2018, *AJ*, 156, 123, doi: 10.3847/1538-3881/aabc4f

The CASA Team, et al., 2022 "CASA, the Common Astronomy Software Applications for Radio Astronomy", *PASP*, 134, 114501. doi: 10.1088/1538-3873/ac9642

Thompson, A. R. 1982, *IEEE Transactions on Antennas and Propagation*, 30, 450, doi: 10.1109/TAP.1982.1142799

Thompson, A. R. 1999, in *Synthesis Imaging in Radio Astronomy II*, ed. Taylor, G. B., Carilli, C. L., Perley, R. A. 1999, *ASP Conference Series*, 11-36

7 APPENDIX A – SITE PROPAGATION PROFILES

The Figures below show terrain and vegetation analysis between several of the test sites and the center of the array.



Figure A1: Rest Area Site, Position 1.2

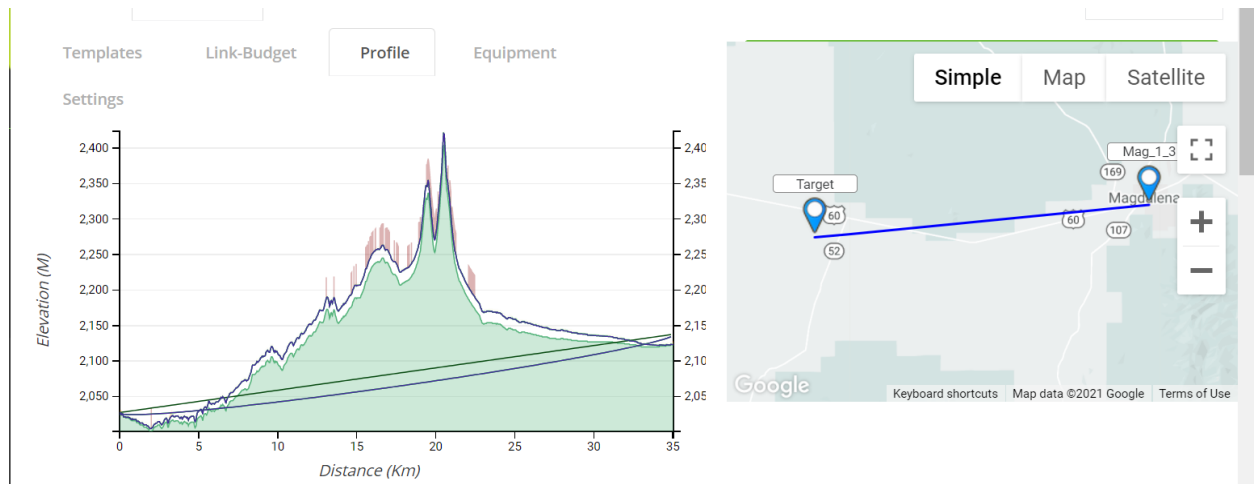


Figure A2: Magdalena Site, Position 1.3

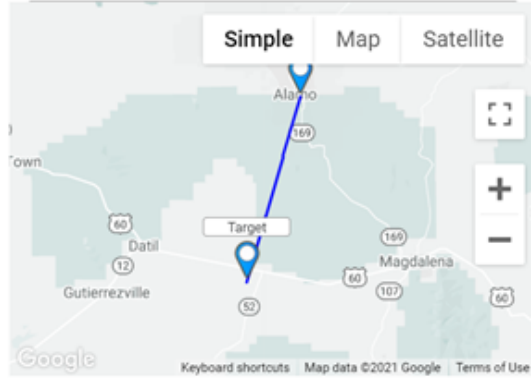
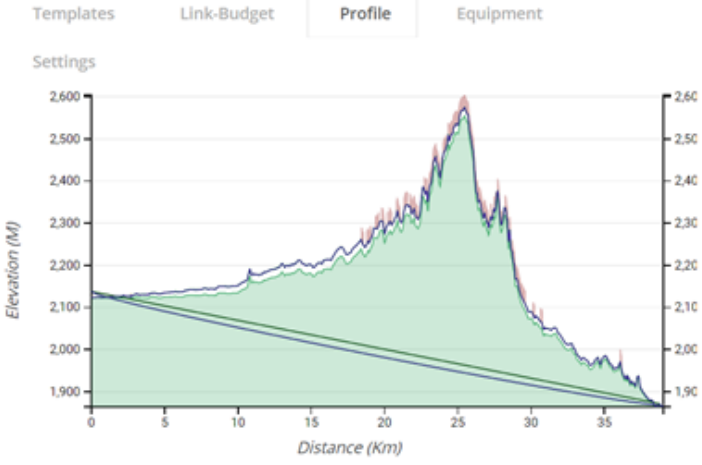


Figure A3: Alamo Site, Position 2.2

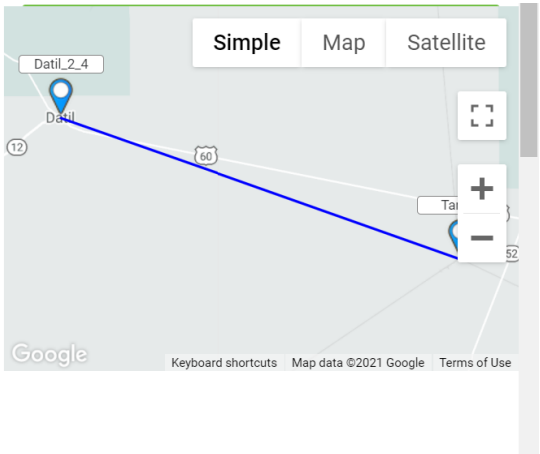


Figure A4: Datil Site 2, Position 2.4

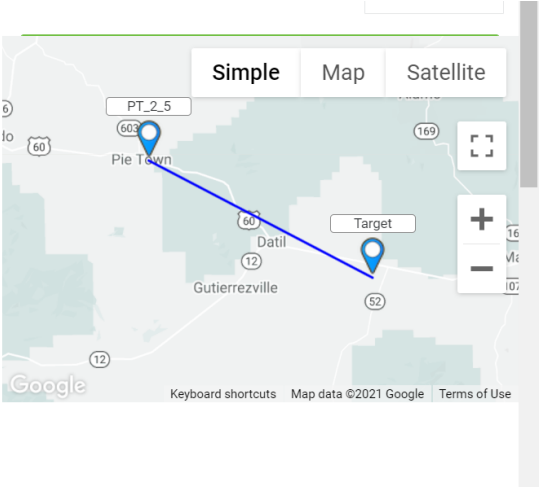
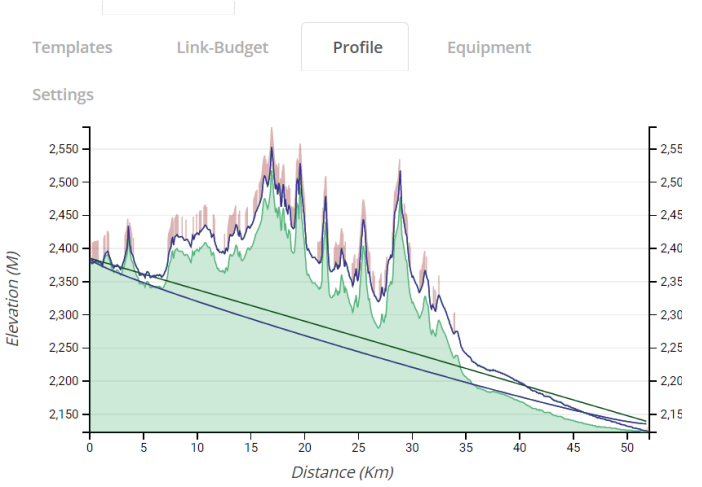


Figure A5: Pie Town Site, Position 2.5